

# Characterization of a carbonate geothermal reservoir using rock-physics-guided deep neural networks

Fabien Allo<sup>1</sup>, Jean-Philippe Coulon<sup>2</sup>, Jean-Luc Formento<sup>2</sup>, Romain Reboul<sup>2</sup>, Laure Capar<sup>3</sup>, Mathieu Darnet<sup>3</sup>, Benoit Issautier<sup>3</sup>, Stephane Marc<sup>3</sup>, and Alexandre Stopin<sup>3</sup>

<https://doi.org/10.1190/tle40100751.1>

## Abstract

Deep neural networks (DNNs) have the potential to streamline the integration of seismic data for reservoir characterization by providing estimates of rock properties that are directly interpretable by geologists and reservoir engineers instead of elastic attributes like most standard seismic inversion methods. However, they have yet to be applied widely in the energy industry because training DNNs requires a large amount of labeled data that is rarely available. Training set augmentation, routinely used in other scientific fields such as image recognition, can address this issue and open the door to DNNs for geophysical applications. Although this approach has been explored in the past, creating realistic synthetic well and seismic data representative of the variable geology of a reservoir remains challenging. Recently introduced theory-guided techniques can help achieve this goal. A key step in these hybrid techniques is the use of theoretical rock-physics models to derive elastic pseudologs from variations of existing petrophysical logs. Rock-physics theories are already commonly relied on to generalize and extrapolate the relationship between rock and elastic properties. Therefore, they are a useful tool to generate a large catalog of alternative pseudologs representing realistic geologic variations away from the existing well locations. While not directly driven by rock physics, neural networks trained on such synthetic catalogs extract the intrinsic rock-physics relationships and are therefore capable of directly estimating rock properties from seismic amplitudes. Neural networks trained on purely synthetic data are applied to a set of 2D poststack seismic lines to characterize a geothermal reservoir located in the Dogger Formation northeast of Paris, France. The goal of the study is to determine the extent of porous and permeable layers encountered at existing geothermal wells and ultimately guide the location and design of future geothermal wells in the area.

## Introduction

The aquifer of the Dogger Formation is the main hot water and heat supplier for approximately 40 low-enthalpy geothermal plants currently operating in the Paris Basin. The success of such geothermal projects relies on the quality of the reservoir (i.e., temperature, porosity, and permeability). If the reservoir properties encountered along the geothermal wells fall short of requirements, the project may not be profitable or, in the worst-case scenario, may need to be abandoned. Although the Dogger Formation has been in use for more than four decades, sources of information from which to infer these key reservoir

characteristics are unfortunately scarce. These sources are mainly limited to wireline logs and cores at the well locations and analysis of rock samples where the formation outcrops at the edges of the basin hundreds of kilometers away from the zone of interest. While seismic data are available, albeit limited to series of old 2D lines, they have so far mainly been used to collect structural information such as depth and thickness of the target interval. While future 3D seismic acquisitions will provide higher-quality data with better lateral coverage, several techniques offer ways to retrieve more information from the existing seismic lines. Extensively used in the oil and gas sector, seismic inversion is a standard way to derive elastic properties from recorded seismic amplitudes and infer rock properties away from well control by using deterministic and statistical relationships between elastic and rock properties. Machine learning techniques based on neural networks have also been used for some time to estimate elastic and rock properties from seismic data. These supervised learning algorithms establish a statistical relationship between log and seismic data at the well locations. The relationship is then applied to the seismic data to predict properties of interest at any location within the seismic survey.

While early neural networks such as probabilistic neural networks have been successful in predicting elastic properties (Hampson et al., 2001), estimating rock properties has proved to be more challenging. Considerable expertise is required to reproduce the combination of highly nonlinear rock-physics theories and convolutional seismic modeling with their relatively simple architecture. More advanced neural network architectures, such as deep neural networks (DNNs) and convolutional neural networks, are actively being developed to address this limitation (Feng et al., 2020) and broaden application in the energy industry. Unfortunately, such state-of-the-art networks require a very large amount of data to be trained, which has so far severely limited their applicability for hydrocarbon and geothermal exploration projects. Although the idea of supplementing synthetic data to augment the size of the training set has been explored several times in the past (Balz et al., 1999), statistical methods have mostly been employed to simulate synthetic pseudowells. There is no guarantee that pseudologs created with these techniques follow the same rock-physics laws as the original logs. As a result, they may not be realistic scenarios away from the existing wells. To address this issue, Downton et al. (2020) introduced a novel hybrid theory-guided approach to the generation of synthetic data, which combines the use of theoretical rock-physics models

<sup>1</sup>CGG Canada Services Ltd., Calgary, Canada. E-mail: fabien.allo@cgg.com.

<sup>2</sup>CGG SA, Massy, France. E-mail: jean-philippe.coulon@cgg.com; jean-luc.formento@cgg.com; romain.reboul@cgg.com.

<sup>3</sup>BRGM, Orléans, France. E-mail: l.capar@brgm.fr; m.darnet@brgm.fr; b.issautier@brgm.fr; s.marc@brgm.fr; a.stopin@brgm.fr.

and statistical simulations. This methodology is applied in our study to generate hundreds of pseudowells to train deep feed-forward neural networks (DFNNs) for deriving the total porosity and volume of clays in the Dogger Formation from recorded 2D full-stack seismic lines. These two rock properties are used to compute the effective porosity, from which an absolute permeability

is derived based on laboratory measurements on core data. Results have highlighted a set of relatively continuous porous and permeable layers that will be considered in the design of future geothermal wells in the area.

### Lithostratigraphic overview of the Dogger Formation

The Dogger Formation of the Paris Basin consists of a predominantly limestone assemblage located between marls from the Lias and Malm epochs. The main reservoir units, illustrated in Figure 1, are found within the upper part of the Dogger Formation and result from the development of shallow and granular carbonate facies during the Bathonian and Callovian ages. The base of the Bathonian is characterized by repeated sequences of marls, bioclastic limestones, and calcarenites as part of a large regression that spans the development of a wide carbonate platform centered in the central and eastern Paris Basin. It consists mainly of oolite shoals (Oolithe Blanche Formation), which are the major productive horizons for geothermal energy. The progressive amalgamation of these shoals resulted in the construction of a large barrier that protected a wide inner ramp to lagoon environment, the expansion of which culminated with the Comblanchien Formation at the end of the Bathonian. This unit hosts a quarter of the productive horizons in oolite-rich levels with a complex diagenetic history. While these reservoir facies are easily identified on well logs and outcrops, the objective of the present study is to establish if the existing poststack seismic lines can help track the lateral extent of these layers away from the existing wells and reveal if the porosity and permeability within the layers are fairly homogeneous.

PERIOD	EPOCH	AGE	FORMATION	FACIES			
				Fore Reef	Reef Bar	Back Reef	Lagoon
JURASSIC	MALM	OXFORDIAN	Marls				
		DOGGER	CALLOVIAN	<i>Dalle Nacrée</i>	A		
	BATHONIAN		<i>Comblanchien</i>	B			
			<i>Oolithe Blanche</i>	C			
			Alternating Limestones/Marls				
	BAJOCIAN		Oolitic Limestone				
			Marls with <i>Ostrea acuminata</i>				
		Entrochal Limestone					

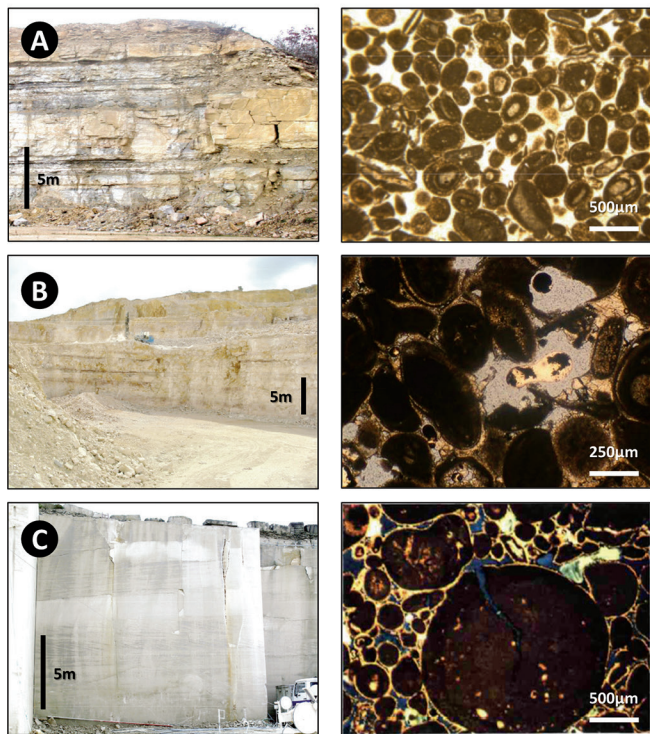
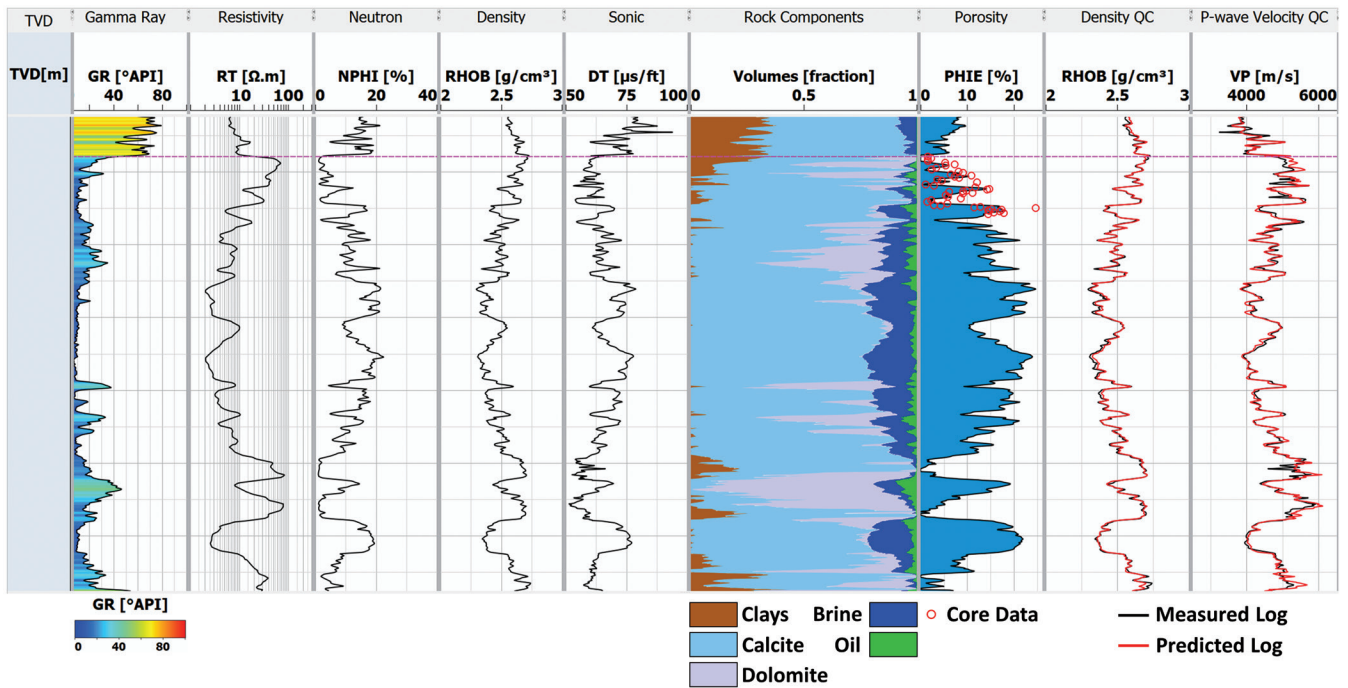


Figure 1. Top: Simplified stratigraphic column of the Dogger Formation located northeast of Paris. Bottom: Analog outcrops and thin sections of the main reservoir units (A, B, and C) located in the Bathonian and Callovian formations southeast of Paris (adapted from Brosse et al., 2010).

### Joint petrophysical and rock-physics analysis

Although 34 wells are in the study area, only four, used for hydrocarbon exploration, have a suite of logs (gamma ray, neutron porosity, density, resistivity, and sonic) suitable for quantitative reservoir characterization. A statistical mineral volume estimation using multilinear regressions is performed based on edited versions of these raw logs. The resulting mineral volumes and porosity logs for one of these wells are displayed in Figure 2. While core measurements are available to calibrate and validate the estimated porosity log, the absence of mud logs and cuttings means the mineral volumes remain more uncertain. To help control the quality of these volumes, a rock-physics-based approach is used. Elastic logs predicted by theoretical rock-physics models from the mineral volumes and porosity are compared with available measured logs. An initial analysis was performed and evaluated based on the match of density and P-wave velocity. While this initial estimation was satisfactory at the time, the subsequent addition of S-wave velocity data from two wells located outside the study area highlighted how the model was unable to reproduce low velocity ratios ( $V_p/V_s$ ) in some intervals of the Dogger Formation. This observation, coupled with the fact that dolomitization in the Comblanchien and *Dalle Nacrée* units has been reported southeast of Paris (Brosse et al., 2010), led to a revision of the rock mineral composition and the introduction of dolomite to better explain the velocity ratio in these intervals. Figure 3 illustrates the main porosity trends observed in the well data. A



**Figure 2.** Petrophysical analysis at one of the exploration wells. Mineral volumes (track 6) and porosity (track 7) are computed from a set of petrophysical logs (tracks 1 to 5) using multilinear regressions. Quality controls include core measurements (red dots in track 7) and elastic log predictions from rock-physics models (red curves in tracks 8 and 9).

large variability is observed in the marls above and below the limestone formation, which can be correlated to a wide range of volume of clays, as highlighted by the rock-physics templates. By contrast, the velocity–porosity relationship in the clean limestone intervals is well defined with very little variation away from the main trend. It can be satisfactorily reproduced by the cemented sandstone model described in Allo (2019). Based on thin-section observations and core-plug analysis, 1% of calcite contact cement is used in the model. The presence of this small amount of cement explains both the high velocities recorded in the limestones and their relatively high porosity. By welding oolites together, the cement contributed to a considerable increase in rock stiffness. At the same time, it prevented much of the mechanical compaction that usually occurs as sediments get buried. The increasing stress applied to the rock during burial, which would relax through a rearrangement of oolites when no cement is present, resulted in pressure dissolution at the contact points and strained oolites that deformed and cracked, as can be seen on the thin section of the Oolithe Blanche Formation in Figure 1c. The match between predicted and measured elastic logs, illustrated in Figure 2, underlines the importance of running a joint petrophysical and rock-physics analysis to produce a consistent set of rock and elastic properties. This ultimately improves the reliability of the rock properties derived from wireline logging through the integration of theoretical rock-physics models instead of purely statistical methods. This also highlights the role of rock physics as a quality-control tool for petrophysical analysis.

### Synthetic data generation

As discussed in the previous section, only four wells have a measured compressional sonic log, which is required to compute a zero-offset synthetic seismic trace. The data from these four

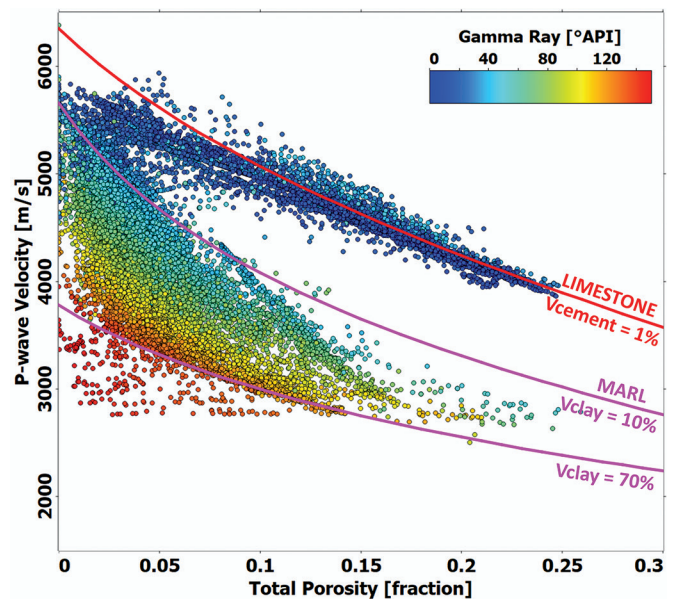


**Figure 3.** Rock-physics templates based on the cemented sandstone model superimposed on log data color coded by gamma ray. The red line, obtained with 1% of cement, fits the main trend observed in the clean cemented limestones. The pink lines, obtained with no cement, delimit marls with an increasing volume of clays (10% for the top line and 70% for the bottom line).

wells only are insufficient to train DFNNs. Therefore, synthetic pseudowells were derived from the existing logs to augment the size of the training data set. Prior geologic knowledge of the area of interest is used to make the pseudowells realistic alternative subsurface scenarios away from the existing wells. Figure 4 illustrates the process followed to create an alternative synthetic petrophysical log from an existing one. Because well logs are nonstationary, each original well is first broken down into intervals

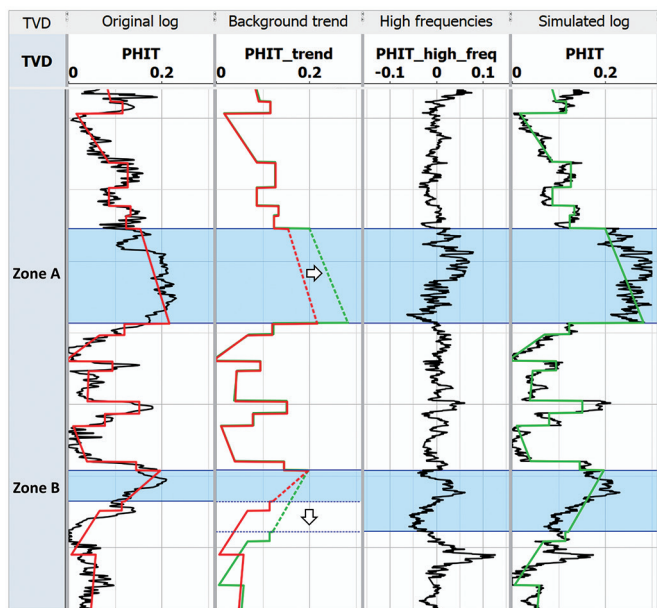


**Figure 4.** Simulation of a realistic synthetic porosity log. A background trend (red curve in track 1) is first extracted from an original log (black curve in track 1) and represents the main evolution in the log with depth. This trend is then modified to represent potential geologic variations away from the original well location. Arrows in track 2 highlight a 30% porosity increase in zone A and a 100% increase in thickness for zone B. High-frequency variations (track 3) based on the original log vertical variability are added to the modified trend (green curve in tracks 2 and 4) to construct the synthetic porosity log (black curve in track 4).

of homogeneous rock properties, within which statistics are considered stationary. The background trend for each rock property input into the rock-physics models is then constructed through a linear regression per interval. Alternative background trends for the synthetic petrophysical logs are obtained through modifications of these original trends. Variations in rock properties can be simulated by shifting or scaling the trend in each interval. The thickness of each layer can also be modified to represent lateral depositional variations. The resulting modified background trends are meant to represent potential variations away from well control and help increase the geologic information contained in the training set. A variographic analysis is then conducted on the original log to estimate how quickly the rock property varies with depth. The resulting vertical variogram is used to constrain the vertical continuity or high frequency of the simulated logs. The high-frequency variations are added to the modified background trends to construct the synthetic petrophysical logs. In this case study, the thickness of the overburden and reservoir layers is modified, as well as the porosity and volume of clays in the reservoir layers. Table 1 summarizes the list of systematic changes applied to each of the original four wells. Altogether, 324 pseudowells were created by the combination of all these scenarios. The simulated petrophysical curves are input into the calibrated rock-physics models to calculate synthetic density and P-wave velocity curves. Synthetic zero-offset seismic traces are obtained by convolving the reflectivity series extracted from the synthetic elastic logs with the statistical zero-phase wavelet derived from the spectral analysis of the seismic lines. The set of synthetic petrophysical logs and seismic traces is used to train the DFNN. None of the original

**Table 1.** List of systematic changes applied to the four original wells to simulate alternative pseudowells. All possible permutations of changes result in the creation of 81 ( $3^4$ ) pseudowells per original well.

Reservoir property		Scenarios
Overburden	Layer thickness	[-5%, 0%, +5%]
Reservoir	Layer thickness	[-5%, 0%, +5%]
	Porosity	[-0.05, 0, 0.05]
	Clay volume	[-0.1, 0, 0.1]

wells are included in the training set, which means they can be used as blind wells to evaluate the quality of the network output. It is important to note that, while the rock-physics models are not directly included in the neural networks, the networks are trained on data computed by the models and therefore indirectly reproduce the theoretical relationships between rock properties and elastic attributes. The networks are referred to as “rock-physics guided” rather than “rock-physics driven” for this reason.

### Evaluation of neural network performance on synthetic data

A DFNN with three hidden layers of 20 nodes is used to estimate total porosity directly from seismic amplitudes. Trained on 75% of the synthetic data, it converges in less than 500 iterations, and a validation error of 16.6% is obtained with the remaining 25% of data. Prior to applying the DFNN to the real seismic lines, tests were run to evaluate its performance in controlled conditions. Synthetic seismic data are derived from an existing 3D model of the subsurface, populated with porosity and volume of clays, and taken as ground truth to which the DFNN results are compared. The calibrated rock-physics models are first applied to compute the acoustic impedance in the 3D model. A zero-offset synthetic 3D seismic cube is then generated by convolving the impedance contrasts with the statistical zero-phase wavelet. In addition to the seismic cube, a low-frequency porosity model is provided as input to the DFNN. This low-frequency model is obtained by applying a high-cut frequency filter (10–15 Hz) to the ground-truth porosity model.

The first test consists of applying the DFNN to the 3D synthetic seismic cube and is designed to evaluate the ultimate performance of the methodology when applied to ideal seismic data free of any acquisition- or processing-related uncertainties. Figure 5 illustrates the porosity obtained in this test and shows that the DFNN manages to qualitatively recover the main variations in rock properties and achieves a reasonable quantitative match with the average mean absolute percentage error (MAPE) computed by equation 1 close to 23.5% in the reservoir interval:

$$\overline{MAPE} = 100 \frac{1}{N_t} \sum_{t=1}^{N_t} \left( \frac{1}{N_i} \sum_{i=1}^{N_i} \left| \frac{P_i - M_i}{M_i} \right| \right), \quad (1)$$

where  $N_t$  is the number of seismic traces,  $N_i$  is the number of samples per trace,  $M_i$  is the model value, and  $P_i$  is the predicted value.

The second test consists of applying the same neural network to a more realistic version of the synthetic seismic data obtained

by adding random noise to the seismic cube used in the first test. To simulate representative noise, the same signal-to-noise ratio of approximately 5 and the same frequency content as observed on the real seismic lines are used. The second test is designed to estimate the extent to which the presence of noise biases the estimated rock properties. Figure 6 illustrates how some of the

noise is carried over in the rock-property estimates because it is interpreted as input signal by the neural network. The average MAPE in this case increases to 40.5%, rendering the estimated rock properties worthless for quantitative use.

Based on this observation, a second neural network is trained on noisy synthetic traces generated from the same set of pseudowells. The role of the third test is to establish if the presence of noise in the training data helps remove some noise from the rock-property estimates. The noisy seismic traces are obtained by adding a random noise to the raw synthetic traces from the pseudowells with the same characteristic signal-to-noise ratio and frequency content as the one added to the 3D synthetic seismic cube. The second neural network outperforms the first when applied to the noisy 3D

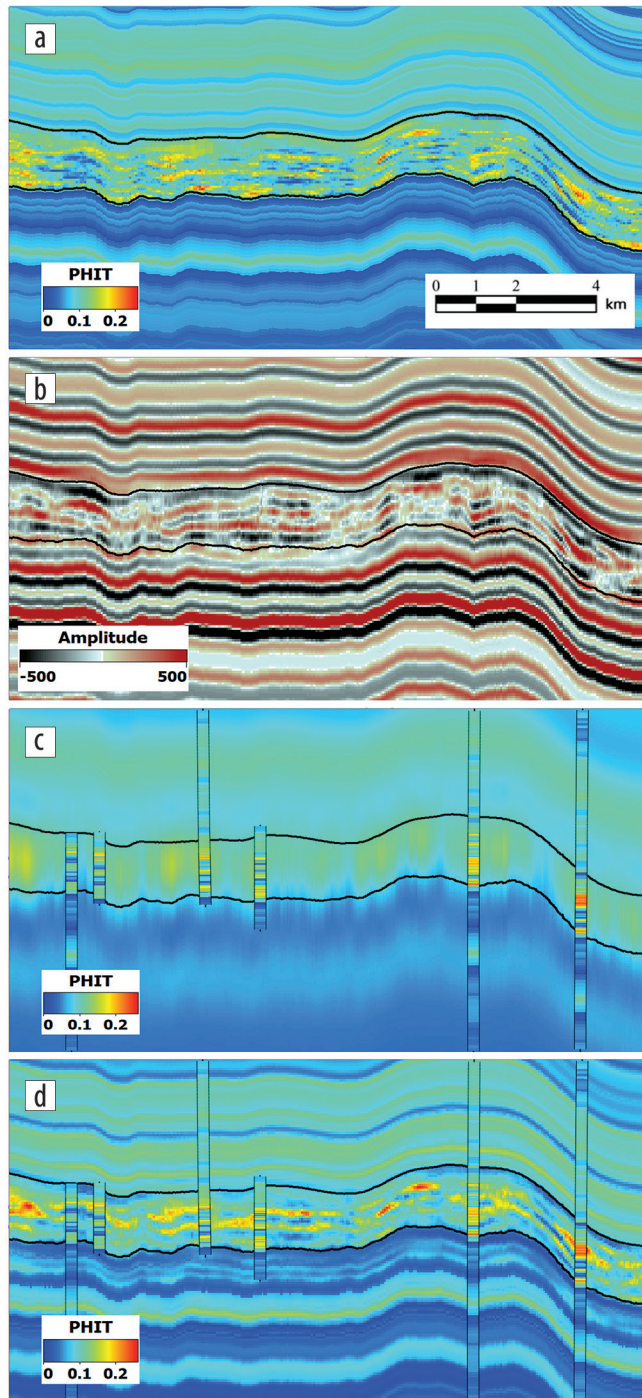


**Figure 5.** Total porosity estimation from ideal seismic data. (a) Porosity model taken as ground truth. The reservoir interval is delimited by the black horizons. (b) Input zero-offset synthetic seismic generated from the true porosity model. (c) Low-frequency porosity model given as input to the DFNN. (d) Porosity estimated by the DFNN trained on ideal synthetic seismic traces created from the pseudowells. The true porosity model is displayed at selected well locations on (c) and (d).

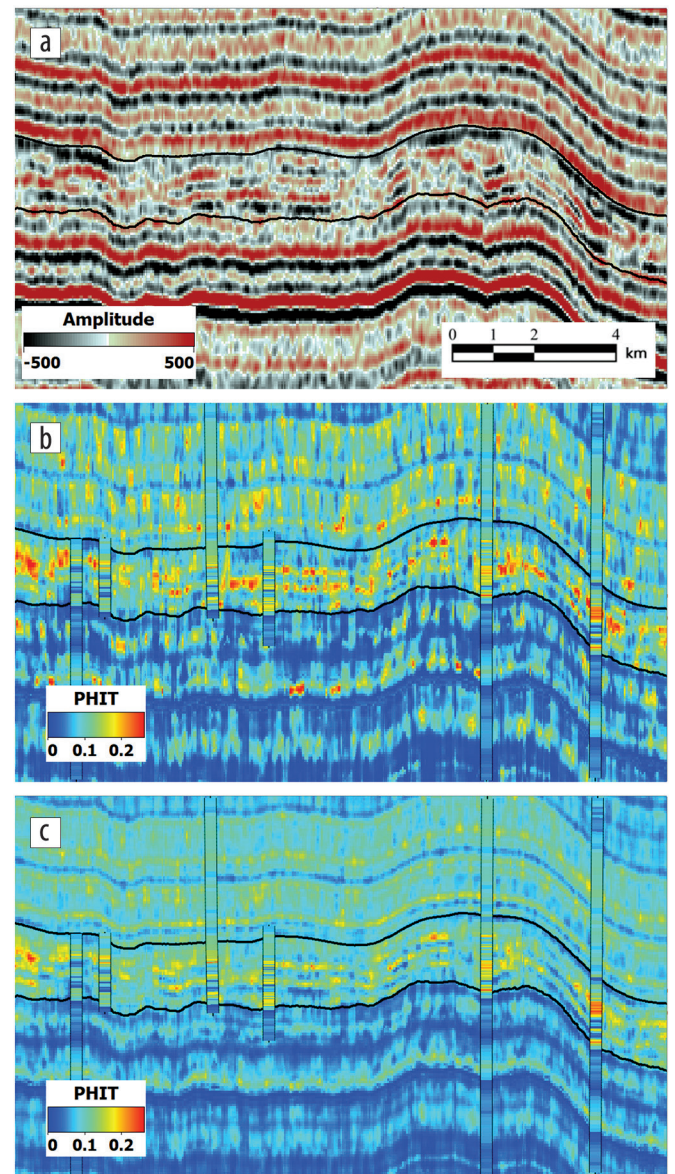


**Figure 6.** Total porosity estimation from noisy seismic data. (a) Input noisy synthetic seismic created by adding random noise to the original synthetic seismic shown in Figure 5. (b) Porosity estimated by the DFNN trained on ideal synthetic seismic traces. (c) Porosity estimated by a DFNN trained on noisy synthetic seismic traces. The true porosity model is displayed at selected well locations on (b) and (c).

synthetic seismic cube with the average MAPE decreasing to 30.9%. While still far from the ultimate performance of the original DFNN, a large portion of the noise present in the input seismic data does not end up in the estimated rock properties. It appears that the noise added to the training set is taken into account by

the second DFNN and used to partly reproduce the observed noise. This third test illustrates the level of uncertainty to be expected in practice when estimating porosity from real seismic data with this type of neural network.

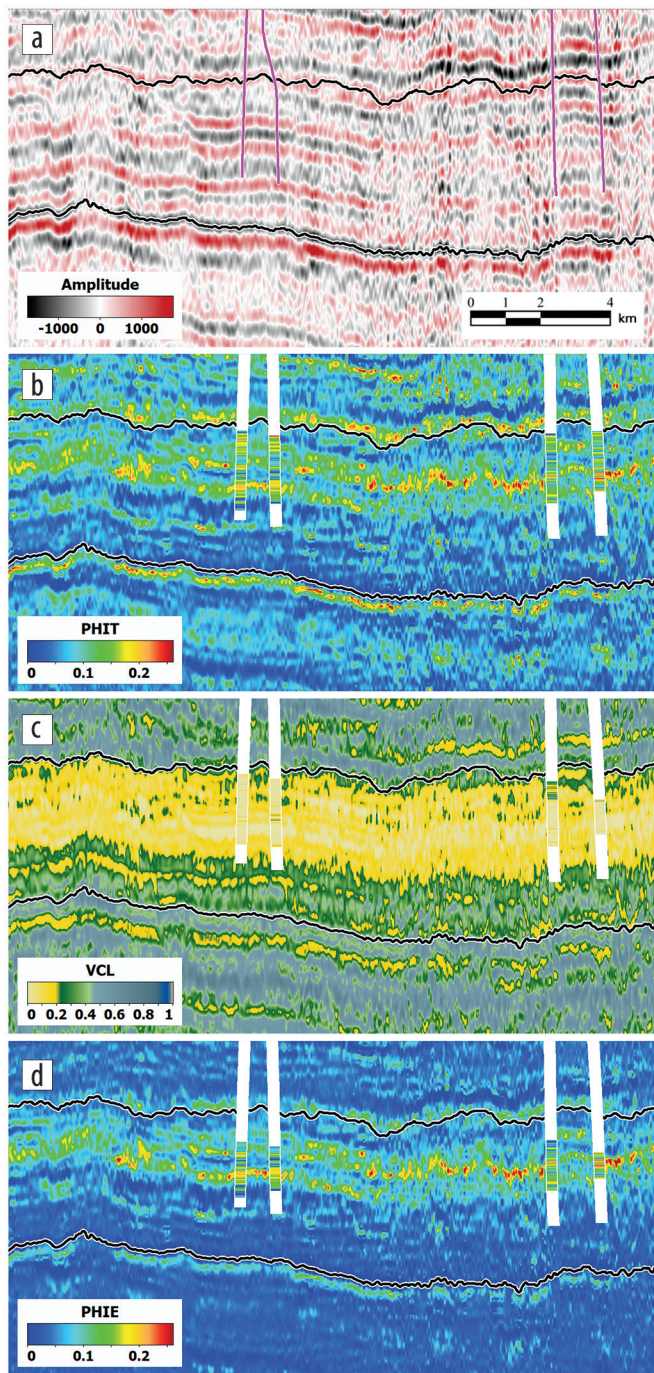
### Application of neural networks to acquired seismic sections

The DFNN trained on noisy synthetic data is applied to five recently reprocessed full-stack seismic 2D lines acquired in the 1980s. While this DFNN derives total porosity from the seismic amplitudes, only effective porosity is of interest for geothermal applications because a fluid needs to be able to circulate in the pore space. For this reason, a volume of clays is estimated with a second DFNN also trained with purely synthetic data. An effective porosity is then derived from the total porosity and clay volume by application of equation 2:

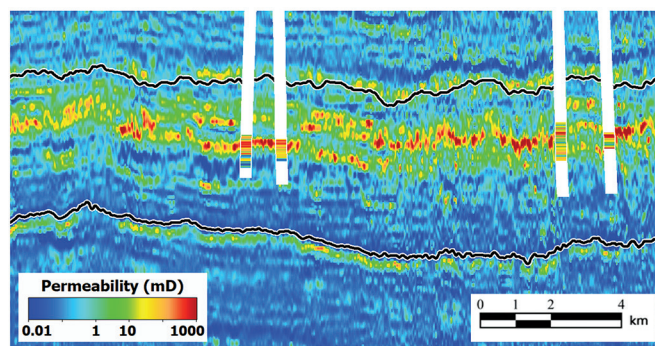
$$\phi_E = \phi_T(1 - V_{clay}). \quad (2)$$

Figure 7 shows the estimated porosities and clay volume along one of the sections crossing the area from west to east. A low volume of clays and some very porous layers are predicted at the top of the Dogger Formation, which is consistent with what is observed on the analog outcrops (Figure 1) and at some nearby geothermal wells. Layers with high total porosity but also high clay content and low effective porosity are predicted immediately above and below the main reservoir interval. These layers correspond to clay-rich marls, with large internal porosity filled with bound formation water, that are of no use for the circulation of geothermal fluids. Without estimating the volume of clays and the effective porosity, these layers could have been misinterpreted and erroneously classified as reservoir facies. Absolute permeability is not estimated directly from the seismic amplitudes but rather computed from the effective porosity by application of equation 3 statistically derived from laboratory core measurements:

$$\log(K) = -2.04 + 30.15\phi_E - 34.16\phi_E^2. \quad (3)$$



**Figure 7.** (a) Input seismic section crossing the study area from west to east. The top horizon represents the top of the Dogger Formation. The bottom horizon corresponds to the top of the marls with *Ostrea acuminata* (Middle Bajocian). (b) Estimated total porosity showing porous layers in the upper part of the Dogger Formation, which correlates with logs from nearby wells. (c) Estimated clay volume confirming that most of the upper part of the Dogger Formation consists of clean limestones. (d) Effective porosity obtained by combining the estimated total porosity and clay volume highlighting layers with high connected porosity.



**Figure 8.** Absolute permeability derived from the estimated effective porosity. Several high-permeability layers are clearly visible in the upper part of the Dogger Formation and represent potential conduits for geothermal fluid circulation. The permeability displayed at the well locations is computed from the effective porosity logs using the same porosity-permeability law.

Figure 8 shows the resulting permeability along the seismic line. Several highly permeable layers can be identified at the top of the Dogger Formation and represent a potential target to consider during the design of future geothermal wells in the area. Variations in effective porosity and permeability are visible in these layers and could be linked to the diagenetic history of this formation, which has seen several phases of dissolution and cementation and resulted in a complex pore-space geometry.

### Neural networks versus seismic inversion

In order to further evaluate the robustness and quality of the estimated rock properties, an acoustic inversion is run on the same 2D seismic lines. Polynomial laws statistically derived from log data are then used to transform the resulting acoustic impedance into total porosity. Because limestones and marls have very distinct elastic behavior, different laws are applied in the reservoir interval (limestones) and in the overburden and underburden intervals (marls). Figure 9 shows a comparison of the total porosities obtained with the DFNN and from the inverted acoustic impedance. A reasonably good qualitative match is observed in the middle of the reservoir interval with similar highly porous layers highlighted by both techniques. However, a clear mismatch is visible at the top and in the lower part of the reservoir interval. Application of the limestone law to clay-rich marls is believed to be the main cause of this substantial porosity overestimation. Such issues are often resolved by running a seismic facies classification prior to applying the facies-dependent impedance-porosity laws. However, a classification solely based on acoustic impedance, the only elastic attribute recoverable from full-stack seismic data, does not reduce the uncertainty significantly in this case due to the large overlap between the impedance distributions of limestones and marls. The use of neural networks turned out to be more user friendly and faster than this multistep inversion-based approach. Another potential advantage of neural networks over seismic inversion in this case is the frequency content of the output porosity. Although the low-frequency model used in both cases is limited to 15 Hz, the porosity obtained with the DFNN has a higher-frequency content. This is mainly due to the different size of convolutional operators used in the two techniques. While the seismic inversion uses a zero-phase wavelet with a breadth of 40 ms (time interval between the center of the two main side lobes), the DFNN is trained with three-point operators equating to a breadth of 6 ms. Therefore, more geologic detail can be resolved from the band-limited seismic data, which is critical for finely layered heterogeneous reservoirs.

### Limitations and pitfalls

While the presented workflow is attractive in its ability to extract geologic information from seismic data, it is important to be aware of its limitations and pitfalls. First, due to the use of band-limited seismic as input data, a low-frequency model of the property of interest needs to be supplied to the neural network to obtain a reliable quantitative estimate. The estimated rock properties are strongly dependent on the input low-frequency model, which represents a severe limitation when well data are very scarce

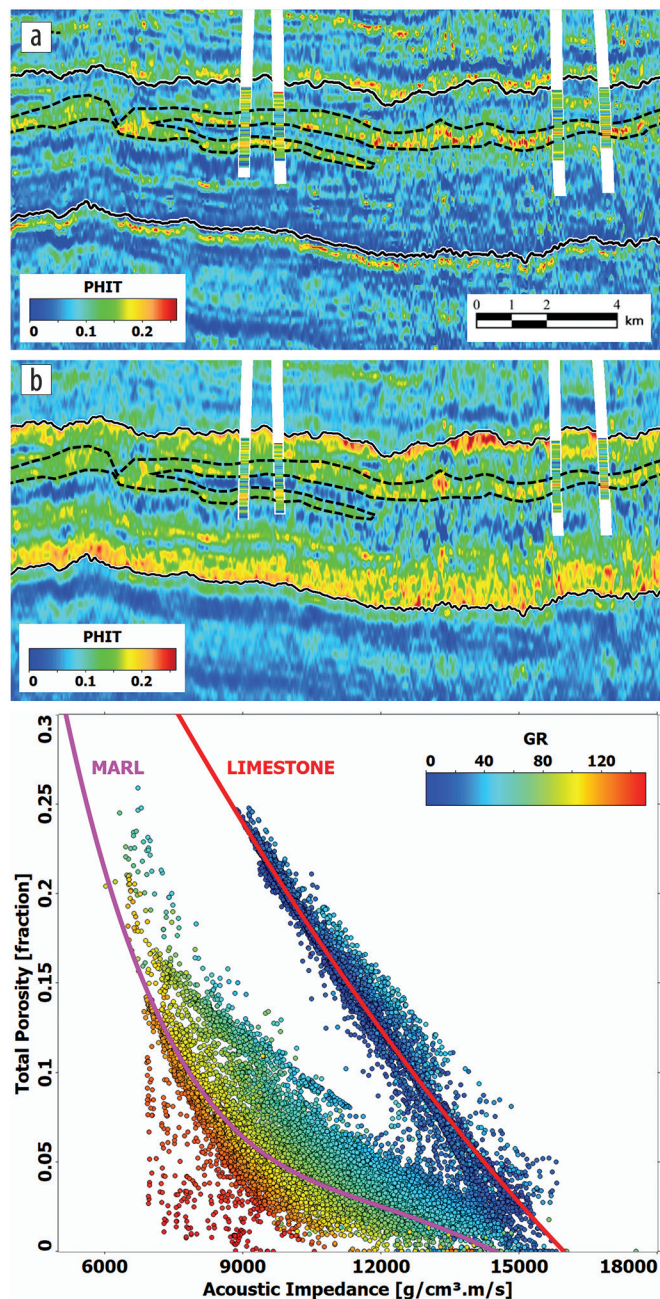


Figure 9. Comparison between total porosities obtained from DFNN and seismic inversion. (a) Total porosity estimated with DFNN. The black dotted lines delimit the highly porous oolitic layers in the upper part of the Dogger Formation. (b) Total porosity derived from inverted acoustic impedance using statistical polynomial laws (bottom) for limestones (red line) and marls (pink line).

or of poor quality. This is the main reason why deriving permeability directly from seismic amplitude was not attempted in this study. Creating a realistic 3D low-frequency permeability model from core data only was not possible. Acquisition of new seismic surveys in the area should alleviate part of this issue by including information at frequencies lower than the current 15 Hz limit and could arguably remove the need for a low-frequency model altogether in the case of broadband seismic acquisition. The use of newly acquired seismic data would also be an opportunity to take into account amplitude variation with offset by feeding partial

stacks or even gathers to the neural networks instead of a single full-stack cube such as in the present study. This has the potential to increase the robustness of rock-property estimates as historically demonstrated with seismic inversion techniques.

Another pitfall that was highlighted during tests to estimate total porosity was the strong sensitivity of the neural networks to the amplitude of the different input data. Any scaling of the input seismic traces results in a scaling of the output rock properties. While conventional seismic well-tie analysis is usually performed to ensure a proper synthetic seismic amplitude calibration, the fact that none of the wells are located on or close to the seismic lines means that no such analysis was possible. The only alternative was to compare the overall energy of the synthetic and real seismic traces in the window of interest via spectral analysis. In addition, while not the case in this study, any significant seismic amplitude variations caused by illumination and/or absorption effects need to be either compensated for or considered when generating the synthetic seismic traces of the training set. Failure to do so would see these amplitude variations translated into erroneous rock-property changes.

To conclude, while generating synthetic pseudowells is an undeniable asset for studies with sparse data, the simulated scenarios need to rely on sound geologic information. Introducing unrealistic property variations results in a synthetic training set that is not representative of the zone of interest and ultimately leads to biased rock-property estimates.

## Conclusion

DFNNs have been applied to predict the porosity and permeability of the Dogger Formation northeast of Paris from 2D reprocessed full-stack seismic lines acquired in the 1980s. The amount of data needed to train such neural networks meant that the original well and seismic data were insufficient to obtain meaningful estimates and required the generation of synthetic data. A set of realistic pseudowells was simulated through the combination of statistical simulations and the application of theoretical rock-physics models. The effective porosity and permeability sections obtained from the neural networks output, while uncertain quantitatively, revealed the position and extent of several layers that could prove to be favorable landing areas for future geothermal wells in the area. Beyond this application to a geothermal study, the ability to train neural networks on

synthetic data makes them a practical alternative to seismic inversion for any type of studies where well-log data are either limited or of poor quality. ■■■

## Acknowledgments

The authors thank the French Geological Survey (BRGM) and CGG for permission to publish this work. We are also grateful to colleagues from CGG GeoSoftware, in particular Olivia Collet and Jon Downton, for support in applying the presented technology. This study is part of a large-scale project financed by BRGM and French Agency for Ecological Transition (ADEME) in the framework of the agreement number 2005C0030 between BRGM and ADEME.

## Data and materials availability

Data associated with this research are confidential and cannot be released.

Corresponding author: [fabien.allo@cgg.com](mailto:fabien.allo@cgg.com)

## References

- Allo, F., 2019, Consolidating rock-physics classics: A practical take on granular effective medium models: *The Leading Edge*, **38**, no. 5, 334–340, <https://doi.org/10.1190/tle38050334.1>.
- Balz, O., F. Pivot, and P. Veeken, 1999, Reservoir characterisation using neural networks controlled by petrophysical and seismic modeling: 61<sup>st</sup> Conference and Exhibition, EAGE, Extended Abstracts, <https://doi.org/10.3997/2214-4609.201407673>.
- Brosse, É., G. Badinier, F. Blanchard, E. Caspard, P. Y. Collin, J. Delmas, C. Dezayes et al., 2010, Selection and characterization of geological sites able to host a pilot-scale CO<sub>2</sub> storage in the Paris Basin (GéoCarbone-PICOREF): *Oil and Gas Science and Technology – Revue d'IFP Energies nouvelles*, **65**, no. 3, 375–403, <https://doi.org/10.2516/ogst/2009085>.
- Downton, J. E., O. Collet, D. P. Hampson, and T. Colwell, 2020, Theory-guided data science-based reservoir prediction of a North Sea oil field: *The Leading Edge*, **39**, no. 10, 742–750, <https://doi.org/10.1190/tle39100742.1>.
- Feng, R., T. M. Hansen, D. Grana, and N. Balling, 2020, An unsupervised deep-learning method for porosity estimation based on poststack seismic data: *Geophysics*, **85**, no. 6, M97–M105, <https://doi.org/10.1190/geo2020-0121.1>.
- Hampson, D. P., J. S. Schuelke, and J. A. Quirein, 2001, Use of multiattribute transforms to predict log properties from seismic data: *Geophysics*, **66**, no. 1, 220–236, <https://doi.org/10.1190/1.1444899>.